IEEE Access
Multidisciplinary | Rapid Review | Open Access Journal

Date of publication xxxx 00, 0000, date of current version xxxx 00, 0000.

Digital Object Identifier 10.1109/ACCESS.2017.DOI

Hybrid SPF and KD Operator-based Active Contour Model for Image Segmentation

ASIF AZIZ MEMON[1], ASIM NIAZ[2], SHAFIULLAH SOOMRO[3], EHTESHAM IQBAL[1], ASAD MUNIR[4] AND KWANG NAM CHOI[1]

[1]School of Computer Science and Engineering, Chung-Ang University, Seoul, Republic of Korea
[2]STARS Team, INRIA, Sophia Antipolis, France.
[3]Department of Computer Science, Quaid-e-Awam University of Engineering, Science and Technology (QUEST), Shaheed Benazirabad, Pakistan
[4]Department of Industrial and Information Engineering, Università degli Studi di Udine, 33100 Udine, Italy

Corresponding author: Kwang Nam Choi (e-mail: knchoi@cau.ac.kr).

This work was supported by the National Research Foundation of Korea (NRF) grant funded by the Korea Government (MSIT) (No.2019R1F1A1062612).

ABSTRACT Image segmentation is a crucial stage of image analysis systems because it detects and extracts regions of interest for further processing, such as image recognition and the image description. However, segmenting images is not always easy because segmentation accuracy depends significantly on image characteristics, such as color, texture, and intensity. Image inhomogeneity profoundly degrades the segmentation performance of segmentation models. This paper contributes to image segmentation literature by presenting a hybrid Active Contour Model (ACM) based on a Signed Pressure Force (SPF) function parameterized with a Kernel Difference (KD) operator. An SPF function includes information from both the local and global regions, making the proposed model independent of the initial contour position. The proposed model uses an optimal KD operator parameterized with weight coefficients to capture weak and blurred boundaries of inhomogeneous objects in images. Combined global and local image statistics were computed and added to the proposed energy function to increase the proposed model's sensitivity. The segmentation time complexity of the proposed model was calculated and compared with previous state-of-the-art active contour methods. The results demonstrated the significant superiority of the proposed model over other methods. Furthermore, a quantitative analysis was performed using the mini-MIAS database. Despite the presence of complex inhomogeneity, the proposed model demonstrated the highest segmentation accuracy when compared to other methods.

INDEX TERMS Active contour, Intensity inhomogeneity, Image segmentation, Region-based, Local and global intensity

I. INTRODUCTION

Image segmentation is a principal research direction in image processing and is widely used in image analysis, medical imaging, and computer vision [1]–[3]. In image segmentation, a given image is divided into several regions with specific characteristics such as color, texture, and intensity levels. Many previous studies have been proposed for solving image segmentation problems, such as threshold-based, supervised learning-based, and non-supervised learning-based methods. The threshold method is based on the assumption that clusters of pixel intensity histograms correspond to a particular object of interest. Deep learning-based image segmentation methods fall under the category of supervised methods and require significant resources and data sets compared to other methods [43].

The widely-used active contour model (ACM) [4]–[9], can successfully manage the topological changes in the contour curves over objects having distinct geometrical shapes. The ACM, initially proposed by Kass et al.[19], can yield a closed and smooth curve to represent the edges of an object while constructing the energy function regarding continuous curves as the independent variable so that the segmentation process calculates the minimum value of the energy function [10]. It can be expressed by calculating the Euler–Lagrange

This article has been accepted for publication in a future issue of this journal, but has not been fully edited. Content may change prior to final publication. Citation information: DOI 10.1109/ACCESS.2020.3034908, IEEE Access

equation of the function. The contour movement depends on the internal and external forces, and the contour over object boundaries stops when the energy reaches a minimum or when both the forces become equal.

ACMs can be divided into two categories: edge-based and region-based. Edge-based ACMs are generally based on the assumption that the gradient information is used to detect edges according to the size of the gradient, thus guiding the evolving contour to move toward object boundaries near the edges of segmented regions [11]–[12]. However, the segmentation results may not succeed when an image is noisy or if the object boundary is weak.

Region-based ACMs can approximate the region of interest (ROI) more precisely and accurately. Region-based methods use regional descriptors, such as intensity and color, to capture ROIs, yielding superior performance in the presence of distorted edges and noise. Chan–Vese (C–V), which is based on the Mumford–Shah model [13], is a widely used region-based ACM model. The C–V [3] model computes the difference between the averages of intensity from the inner and outer regions. This difference is used to drive the contour toward object boundaries. Because region-based models are based on the assumption that the ROI is comprised only of a homogeneous intensity, this limits the model's performance over inhomogeneous images. Furthermore, its non-convex function is fixed to the local minima, thereby increasing the computational cost.

Dealing with the intensity inhomogeneity in images and developing a robust method to segment inhomogeneous images is challenging. Li et al. presented their local binary fitting (LBF) [4] model based on the standard LBF model [4] to address this limitation. The LBF model extracts local image information using a localized convolutional kernel function. A scalable parameter is used to extract image features, while local image information controls the curve evolution [14]–[17]. Another local ACM used for the segmentation of inhomogeneous images was proposed by Zhang et al. [23]. This method uses local image fitting energy to segment inhomogeneous images using local image information. When the amount of overlap in the inhomogeneous image between the background or foreground intensity distributions is hard to be estimated [35]-[38]. The local image information is extracted by a local image fitting energy function interpreted as the difference between the fitting and the original input images. A region-based ACM using a signed pressure force function was proposed [24]. This model uses global intensity means for the detection of ROI. The expensive reinitialization is avoided using a Gaussian regularization function.

Li et. al. proposed their model comprising a variational level set with bias correction (VLSBC) for the segmentation of images corrupted with bias conditions [25]. This method computes the bias field and then corrects it to achieve a smoothened final level set. Zhang et al. [23] proposed a local statistical ACM (LCASM) targeting inhomogeneous image objects in images. The LCASM model's objects of interest are Gaussian distributions of different means and variances. This method uses a window to map the original image into a new domain where inhomogeneous intensity Gaussian distribution spreads more evenly. This transformed Gaussian distribution implies that adaptive estimation can be performed by multiplying both the bias field and the original image within the window. The model then defines a statistical function for each local region, combining the bias field, the level set function, and the estimated true signal.

Zhang et al. proposed a signed pressure force (SPF) [20] to segment images. The SPF computes the average values of the global foreground and background regions as the comparison center and exploits the differences among image intensities. The SPF replaces the edge stopping function in the geodesic ACM and its level set evolution. A Weighted Hybrid Region-based SPF (WHRSPF)[39] normalized the evolving curve's global intensity by the inner and outer region's coefficient. An adaptively weighted global region-based SPF (GRSPF) function defines the global pixel information to avoid the parameter setting's difficulty and improves the ability of intensity inhomogeneity. Global and Local signed energy-based pressure force (GLSEPF) [40] was proposed to improve the initial curve's robustness and compute the pixel-by-pixel energy difference within the local region. It helps to handle the noise in inhomogeneous images and intensity. The regularization term and penalty term were used to avoid the re-initialization process. A global weighted SPF (GWSPF) and the local weighted SPF (LWSPF) [41] were proposed to improve the segmentation performance by the difference of information of the inner and outer regions.

In this paper, a hybrid ACM based on an SPF function parameterized with a kernel difference (KD) operator is defined. An SPF function includes information for both the local and global regions, making the proposed model independent of the initial contour position. An optimal KD operator is used to capture weak edges of the object boundary and improve the segmentation accuracy. A parameterized weight coefficient is used to capture inhomogeneous objects in images to improve the sensitivity of the proposed model.

The organization of the paper is as follows. The theoretical foundations are briefly discussed in Section II. The proposed research methodology is explained in Section III, and the results with synthetic and real-life images are explained in Section IV. Section V presents the quantitative comparison of the proposed method with the previous state-of-the-art level set methods using Synthetic color images and the mini-MIAS database.

II. BACKGROUND

A. MUMFORD SHAH ENERGY MODEL

Mumford and Shah [13] proposed their energy model for image segmentation and formulated the segmentation problem as finding an optimal piece-wise smooth approximation function u of the input image $I(x)$. This approximation function varies smoothly within each sub-region Ω_i of the image domain $\Omega_i \subset R^2$. The Mumford–Shah energy function is

understood as the following:

$$E_{MS} = \lambda \int_{\Omega} (I(x) - u(x)^2)dx + v \int_{\Omega\setminus} C|\nabla u|^2 dx + \mu Length(C), \tag{1}$$

where μ and $v \geq 0$ are the constant parameters. $|C|$ represents the contour length. The non-convexity of the energy function in (1) makes it difficult to be minimized.

B. CHANVESE ENERGY MODEL

Chan and Vese (C–V) created their ACM based on the Mumford–Shah model [3]. Suppose $I(x) : \Omega \rightarrow R^2$ is an input image, $\phi : \Omega \rightarrow R$ is the level set, and C is the closed curve. The C–V model energy function is defined as

$$E_{CV} = \lambda_1 \int_{\Omega 1} |I(x) - m_1|^2 H_\epsilon(\phi)dx + \lambda_2 \int_{\Omega 1} |I(x) - m_2|^2 (1 - H_\epsilon(\phi))dx + \mu \int_{\Omega} |\delta H_\epsilon(\phi)|^2 dx + v \int_{\Omega} H_\epsilon(\phi)dx \tag{2}$$

where $H_\epsilon(\phi)$ represents the Heaviside function with the following relationship :

$$H_\epsilon(\phi) = \frac{1}{2} + \frac{1}{\pi} arctan(\frac{\phi}{\epsilon}) \tag{3}$$

In (2), μ, v, λ_1, and λ_2 are the fixed positive parameters. ϵ controls the width of the Heaviside function. The Euclidean length of curve C is scaled with the parameter μ while parameter v scales the area term in the C–V [3] model. m_1 and m_2 are the average of the intensities inside and outside contour C, respectively. By minimizing (2) with respect to ϕ, the following level set function is obtained:

$$\frac{\partial \phi}{\partial t} = \delta_\epsilon(\phi)(\lambda_1 (I(x) - m_1)^2 + \delta_\epsilon(\phi)\lambda_2 (I(x) - m_2)^2 + \delta_\epsilon(\phi)\mu div\left(\frac{\nabla \phi}{|\nabla \phi|}\right) - \delta_\epsilon(\phi)v \tag{4}$$

where $\delta_\epsilon(\phi)$ is the Dirac delta function defined as:

$$\delta_\epsilon(\phi) = \frac{\epsilon}{\pi(\phi^2 + \epsilon^2)} \tag{5}$$

where ϵ corresponds to the width of the Dirac delta function. m_1 and m_2 in (2) and (4) are the average intensity means inside and outside the contour and are respectively defined as

$$m_1 = \int_{\Omega} \frac{I(x)H_\epsilon(\phi)}{H_\epsilon(\phi)}, \tag{6}$$

$$m_2 = \int_{\Omega} \frac{I(x)(1 - H_\epsilon(\phi))}{(1 - H_\epsilon(\phi))} \tag{7}$$

In the C–V [3] model, the difference between m_1 and m_2 should be significant enough to attract the contour to the desired boundary of the object of interest. The C–V [3] model was designed based on the assumption that images comprise only homogeneous regions, which limits this method in situations with inhomogeneous images.

C. LOCAL BINARY FITTING ENERGY MODEL

Li et al. proposed a solution to address the limitations of the C–V [3] model in their LBF model [4], which can use images corrupted by inhomogeneity. The LBF model introduces a binary fitting energy function in a local region specified by a Gaussian kernel [4]. The LBF energy model is defined as

$$E_{LBF} = \lambda_1 \int_{\Omega} K_\sigma(x - y)|I(y) - f_1(x)|^2 H_\epsilon(\phi))dydx + \lambda_2 \int_{\Omega} K_\sigma(x - y)|I(y) - f_2(x)|^2 (1 - H_\epsilon(\phi)))dydx \tag{8}$$

where $I(x) : \Omega \rightarrow R^2$ is the input image, K_σ is a Gaussian kernel, and f_1 and f_2 are the two smooth spatially- varying local intensity means of the inner and external regions of the contour C. λ_1 and λ_2 are the positively fixed parameters. We added the distance regularizing term found in Li et al.'s variational level set formulation [6] to penalize the deviation of the level set function ϕ from a signed distance function to ensure the stable evolution of the level set function ϕ. The deviation of the level set function ϕ from a signed distance function is characterized by the following integral:

$$P(\phi) = \int_{\Omega} \frac{1}{2}(|\partial \phi(x)| - 1)^2 dx \tag{9}$$

The length of the zero-level curve (surface) of ϕ is required to regularize the zero-level contour of ϕ, given by

$$L(\phi) = \int_{\Omega} \epsilon(\phi(x))|\partial \phi(x)|dx \tag{10}$$

In the LBF model, $C \subset \Omega$ is represented by the zero-level set of the Lipschitz function $\phi \subset R$ [4]. Minimizing (8) with respect to ϕ, the gradient descent flow equation is defined as

$$\frac{\partial \phi}{\partial t} = -\left(\lambda_1 e_1 - \lambda_2 e_2\right)\delta_\epsilon(\phi) + \mu P(\phi) + vL(\phi) \tag{11}$$

where μ and v are nonnegative constants . In (11), e_1 and e_2 are respectively defined as

$$e_1(x) = \int_{\Omega} K_\sigma(x - y)|I(y) - f_1(x)|^2 dy, \tag{12}$$

and

$$e_2(x) = \int_{\Omega} K_\sigma(x - y)|I(y) - f_2(x)|^2 dy, \tag{13}$$

f_1 and f_2 are respectively defined as

$$f_1(x) = \frac{K_\sigma[I(x)H_\epsilon(\phi)]}{K_\sigma H_\epsilon(\phi)}, \tag{14}$$

and

$$f_2(x) = \frac{K_\sigma[I(x)(1 - H_\epsilon(\phi))]}{K_\sigma(1 - H_\epsilon(\phi))}, \tag{15}$$

The standard deviation σ of the Gaussian kernel is a scaling parameter that controls the region's scalability from the small neighborhood to the full image. The limitation of this model is its dependence on the initial contour position to avoid local minimums due to the localization property of the Gaussian kernel.

This article has been accepted for publication in a future issue of this journal, but has not been fully edited. Content may change prior to final publication. Citation information: DOI 10.1109/ACCESS.2020.3034908, IEEE Access

D. SBGFRLS ENERGY MODEL

The selective binary and Gaussian filtering regularized level set (SBGFRLS) model was proposed based on the traditional C–V and geodesic active contour (GAC) MODELS, having the advantages of both [20]. a SPF function used to substitute ESF in the GAC model; the SBGFRLS formulation can be expressed as

$$\frac{\partial \phi}{\partial t} = spf(I(x)).|\nabla \phi|.\alpha, \tag{16}$$

where $spf(I(x))$ is an SPF function in Equation (16), which is defined as

$$spf(I(x)) = \frac{I(x) - \frac{m_1+m_2}{2}}{max(|I(x) - \frac{m_1+m_2}{2}|)'} \tag{17}$$

where m_1 and m_2 represent the gray mean values of the inside and outside of the contour regions and are computed using Equations (6) and (7), respectively. The SBGFRLS model reduces the cost of the expensive re-initialization process of the traditional level set method, which is more efficient than other traditional models. The contour's evolution stops without any prior training over the blurred edges. However, the model assumes that the region to be segmented is homogeneous, which occasionally holds in general clinical cases. The detection accuracy can be decreased significantly, when facing heterogeneous intensity distributions, because the fundamental assumption is violated [21],[22]. Moreover, the SBGFRLS model can become trapped in a local minimum without proper initialization, resulting in poor segmentation performance [26–28],[32].

E. LOCAL IMAGE FITTING ENERGY MODEL

The local image fitting (LIF) energy model was proposed to minimize the difference between the fitted and input images [17]. This model is based on the piece-wise smooth assumption that the internal and external regions can reconstruct input images I in a local region. The LIF energy model is defined as

$$E_{LIF} = \frac{1}{2}\int_{\Omega} |I(x) - I_{LIF}(x)|^2 dx, \tag{18}$$

where I_{LIF} accounts for the local fitted image, which is defined as

$$I_{LIF}(x) = f_1(x)M_1 + f_2(x)M_2 \tag{19}$$

$M_1 = H_\epsilon(\phi)$ and $M_2 = 1 - H_\epsilon(\phi)$ and f_1 and f_2 are the local intensity means in the input images in (14) and (15). Using calculus of variations, (18) is minimized to

$$\frac{\partial \phi}{\partial t} = (I(x) - I_{LIF}(x))(f_1(x) - f_2(x))\delta_\epsilon(\phi), \tag{20}$$

where $\delta_\epsilon(\phi)$ is the regularized Dirac delta function. This model achieves accuracy similar to that of the LBF [4] model. However, the LIF [17] model ignores some details of small objects because of the Gaussian filter, resulting in inadequate image segmentation.

F. VLSBC ENERGY MODEL

Li et al. [25] proposed the variational level set with bias correction (VLSBC) model. This method computes the bias field of images and then attempts to correct it to ensure an image's smoothness through the data term in the energy model. The VLSBC model [25] is inspired by the retinex model to describe inhomogeneous images as

$$I(x) = b(x)J(x) + n(x) \tag{21}$$

where $I(x)$ is the input image, $J(x)$ is the true image independent of the inhomogeneity, and $n(x)$ is the image noise. The true image $J(x)$ is assumed to be constant within each object in the image and is defined as

$$J(x) \approx \sum_{i=1}^{N} c_i M_i, \qquad for\ x \in \Omega_i \tag{22}$$

The K-means clustering function is

$$E \approx \sum_{i=1}^{N} \int \left(\int K_\sigma(x-y)|I(y) - b(x)c_i|^2 M_i(\phi) dy \right) dx \tag{23}$$

where M_i is the characteristic membership function based on the regularized Heaviside function. If the image domain is divided into two regions Ω_1, Ω_2, and M_i are defined as $M_1 = H_\epsilon(\phi)$ and $M_2 = 1 - H_\epsilon(\phi)$, then c_i and $b(x)$ are expressed as

$$c_i = \frac{\sum_{i=1}^{2} K_\sigma * [I(x)c_i M_i(\phi)]}{\sum_{i=1}^{2} K_\sigma * [c_i^2 M_i(\phi)]}, \tag{24}$$

and

$$b(x) = \frac{\int K_\sigma * [I(x)b(x)M_i(\phi)]}{\int K_\sigma * [b(x)^2 M_i(\phi)]} \tag{25}$$

This method produces suitable results for inhomogeneous image segmentation. However, its dependence over the initial contour position limits its performance.

III. THE PROPOSED METHOD

The proposed ACM constructs a driving force based on the information in the region of the image. By combining local and global SPF functions in which the region information modulates pressure force, a hybrid SPF function is proposed. The proposed hybrid SPF function helps the proposed model to be independent of the initial contour position. Furthermore, an optimal KD operator is used to capture the weak edges of the object boundary.

A. UPGRADED SPF FUNCTION

1) Global SPF

The inclusion of the SPF function in the proposed method contributes to the global information of an image I. The global fitting information is defined as

$$s = H_\epsilon(\phi).*(I - m_1) + (1 - H_\epsilon(\phi)).*(I - m_2), \tag{26}$$

where H_ϵ is the regularized Heaviside function defined in Equation (3), .* describes the matrix multiplication, and m_1

This article has been accepted for publication in a future issue of this journal, but has not been fully edited. Content may change prior to final publication. Citation information: DOI 10.1109/ACCESS.2020.3034908, IEEE Access

and m_2 are the averages of the intensities defined in Equations (6) and (7), respectively. Based on the above defined global fitted image, the upgraded SPF function is defined as

$$spf_g(I(x)) = \frac{I(x) - s(x)}{max(|s(x)|)} \tag{27}$$

2) Local SPF

The local SPF function is introduced as the coefficient of local internal and external regions to enable the model to use inhomogeneous images and computed as

$$spf_l(I(x)) = \frac{(I(x) - \frac{f_1+f_2}{2})}{max(|I(x) - \frac{f_1+f_2}{2}|)} \tag{28}$$

where f_1 and f_2 are the two smooth, specially varying local intensity means of the internal and external regions defined in (14) and (15).

3) Upgraded SPF

We built an upgraded SPF function by using the global spf_g and local spf_l defined in (27) and (28) to segment the weak boundary in an inhomogeneous image .

$$spf_{Up}(I(x)) = w(spf_l(I(x))) + (1-w)spf_g(I(x)) \tag{29}$$

w is a weighting parameter that adjusts the local and global spf energies. Where w is the average of $(C_N).(1 - C_N)$; the intensity changes rapidly within the local window, which is denoted by C_N, where the local window size N defined as $C_N = (I_{max} - I_{min})/I_g$. The values of Both w and $(1 - w)$ are between 0 and 1. I_{max} is maximum intensity, and I_{min} is the minimum intensity within the local window, respectively. The intensity level of an image is usually 255, denoted by I_g. The w is based on the degree value of an image inhomogeneity, where a lower value implies a lower degree and higher degree of inhomogeneity value implies a higher degree. Substituting the upgraded SPF function (29) in Equation (16), the evolution equation of the upgraded SPF function is defined as

$$\frac{\partial \phi}{\partial t} = spf_{Up}(I(x)).b|\nabla \phi| \tag{30}$$

The balloon force is defined by b, which is used to control the contour evolution process with shrinkage or expansion over the image. In this paper, we adopted the balloon force [33] to change the evolution rate of the level set function, which is defined as

$$b = m_1 + m_2. \tag{31}$$

Because the SPF function is less sensitive to the initialization location, the upgraded SPF function avoids the reinitialization step.

B. KERNEL DIFFERENCE

In this paper, images could be obtained by subtracting two filtered images to separate the noise and background from the desired object [18]. By the convolution of the original image $I(x, y)$, the KD can be defined with two standard deviations σ_1 and σ_2.

$$K * I(x, y) = (k_{\sigma 1} - k_{\sigma 2}) * I(x, y), \tag{32}$$

where K is the KD with two standard deviations k_1 and k_2. By convolutionizing the original image, the KD is further defined as

$$k_{\sigma 1} * I(x, y) - k_{\sigma 2} * I(x, y), \tag{33}$$

If the image is corrupted with intensity inhomogeneity and noise, it becomes highly sensitive to the gray changes because the kernel operator is a second-order differential operator. An edge energy term can be constructed to solve these problems, defined as

$$\begin{aligned} E_K(g) = \int \int_{\omega} & w((k_{\sigma 1} - k_{\sigma 2}) * g - 0)^2 \\ & + (g - \alpha(k_{\sigma 1} - k_{\sigma 2}) * I(x, y))^2 dxdy, \end{aligned} \tag{34}$$

where the optimal kernel operator is represented by g, and w is a positive weighting coefficient used to stabilize the first and the second terms. If the image noise is greater, then the value of w is higher. The α is used to enhance or preserve the object edges when α is greater than 1 or equal to 1. The boundaries of an inhomogeneous image are enhanced when g approaches zero. Equation (34) is used to preserve the edges of the image, and both terms are fitting terms used to measure the proximity and approximation among the original kernel operator, zero plane, and optimal kernel operator.

$$\frac{\partial g}{\partial t} = w(k_{\sigma 1} - k_{\sigma 2}) * g - (g - \alpha(k_{\sigma 1} - k_{\sigma 2}) * I(x, y)) \tag{35}$$

Equation (35) was obtained by iterating the original kernel operator 100 times. The adopted parameters and corresponding values were set as w=3.2, α=1, σ_1=3.5, σ_2=1.5, and $\delta t = 0.01$. We used the zero-level set function to represent the closed contour C. Therefore, an energy function was proposed:

$$E_k(\phi) = g(\phi) = \int \int_{\omega} H(\phi) g(x, y) dxdy, \tag{36}$$

$H(\phi)$ is Heaviside function defined in (3). By minimizing Equation (36) with respect to ϕ, the corresponding gradient descent flow equation was obtained as follows:

$$\frac{\partial \phi}{\partial t} = \delta_\epsilon(\phi) g \tag{37}$$

where $\delta_\epsilon(\phi)$ is the Dirac function defined in (5), and g is the optimal kernel operator defined in (35).

C. ACM BASED ON KERNEL DIFFERENCE AND UPGRADED SPF

The KD helps to detect edges in the image segmentation process when the object edges are weak. Moreover, the upgraded SPF function is used to construct global image information and effectively processes inhomogeneous images through local image information. We proposed a model that

This article has been accepted for publication in a future issue of this journal, but has not been fully edited. Content may change prior to final publication. Citation information: DOI 10.1109/ACCESS.2020.3034908, IEEE Access

Table 1. The default parameters

Parameters		
Name	Symbol	Value
Gaussian kernel	σ	5.0
Initial level set	λ_1	1
Initial level set	λ_2	1
Time step	Δt	0.1
p-Laplace regularization	μ	1.0
Length term	v	0.01x255x255
Weight	w	0.1/10^5

can process inhomogeneous images with weak edges and reduce the initialization process on the initial contour location with minimum iterations. After combining the upgraded SPF function (30) with KD (37), the newly proposed level set equation is defined as

$$\frac{\partial \phi}{\partial t} = \lambda \delta_\epsilon(\phi) g + (1-\lambda) spf_{Up}(I(x)).b|\nabla \phi| \tag{38}$$

where λ is a positive parameter. Equation (38) defines the proposed level set method that accurately deals with the segmentation problem of weak edges in intensity inhomogeneous images and deals with over-segmentation. Furthermore, the proposed level set method overcomes models that are sensitive to noise and the initial contour position. Finally, iterative steps for the proposed method are summarized as follows.

(1) Initialize level set function ϕ and set the constant functions as the initial contour.
(2) Compute the optimal KD using Equation (35), (35) and (37).
(3) Compute m_1 and m_2 using Equations (6) and (7), respectively.
(4) Compute $H_\epsilon(\phi)$ and $\delta_\epsilon(\phi)$ using Equations (3) and (5), respectively.
(6) Calculate $spf_g(I(x))$ and $spf_l(I(x))$ using Equations (27) and (28), respectively.
(7) Calculate the level set evolution using Equation (38).
(8) Regularize the level set function with the special Gaussian filter, i.e. $\phi = \phi * G_\sigma.(k = 3, \sigma = 3)$.
(9) Verify where contour evolution is converged; if not, return to Step (2).

IV. RESULTS

The proposed method was tested on various synthetic and real images to assess the accuracy levels and computational times. The implementation used MATLAB 2018R in a Windows 10 environment and an Intel Core-i7 3.40 GHz processor with 16 GB of RAM. All default parameters used to segment the inhomogeneous intensity images with the proposed method are defined in Table 1.

A. SYNTHETIC AND REAL IMAGES

Figure 1 illustrates the synthetic and medical images with different intensity inhomogeneity segmentation results using the proposed method. The first column illustrates the original images with different initial contour positions, the second and third columns illustrate the contour moving toward the object rapidly within a few iterations, and the fourth column illustrates the segmentation results of the proposed method. Accordingly, the proposed method is independent of the initial contour position and achieves superior segmentation with fewer iterations. Figure 2 illustrates the medical images used to verify the proposed method's accuracy and time efficiency. The proposed method fitted the contour smoothly with a minimum number of iterations. Figure 3 illustrates the contour evolutions for different initial contour positions with different contour sizes and shapes to validate the proposed method's performance. The first and third columns illustrate the original images with different initial contour positions while columns 2 and 4 present the final segmentation results.

Figure 4 illustrates the segmentation results when using the proposed method on synthetic images; these results were compared with those of previous methods. The first column illustrates the original images with different initial contour positions, column 2 presents the results of the LBF [4] model, columns 3 and 4 present the results of the LIF [17] and VLSBC [25], column 5 illustrates the results of Min et al.'s [29] Method, column 6 illustrates the results of the FRAGL [30] method, column 7 illustrates the results of the LIFDG [31] model, and column 8 illustrates the proposed method's results. The results demonstrate the improved contour evolution of the proposed method compared to the previous methods; however, the results are inaccurate due to image noise and weak object edges.

The proposed method is further compared with SPF methods, WHRSPF [39], and GLSEPF [40] to show the proposed method's robustness. Figure 5 illustrates the synthetic image with different intensity inhomogeneity segmentation results using WHRSPF [39], GLSEPF [40], and the proposed method. The first and Forth column shows the original image with initial contour. Row one shows the results of WHRSPF [39]; the contour is not moving towards the properly. Row two shows the results of GLSEPF [40]; the contour is moving towards the object smoothly. However, the proposed method shows the curve evolution process's smoothness and efficiency than the WHRSPF [39] and GLSEPF [40].

B. NOISE SENSITIVITY ANALYSIS

We have used the Jaccard Similarity (JS) method to perform the noise sensitivity evaluation. JS is used to understand the similarity between the segmentation results of the given images. Two types of artificial noises are used: Salt Pepper and Gaussian. The mathematical representation of the JS metric is written as

$$JS(A,B) = \frac{|A \cap B|}{|A \cup B|}, \tag{39}$$

where A and B represent the segmentation results and ground truth in this experiment.

Figure 6 shows the segmentation results of different images with different levels of Salt & Pepper noise. The top

This article has been accepted for publication in a future issue of this journal, but has not been fully edited. Content may change prior to final publication. Citation information: DOI 10.1109/ACCESS.2020.3034908, IEEE Access

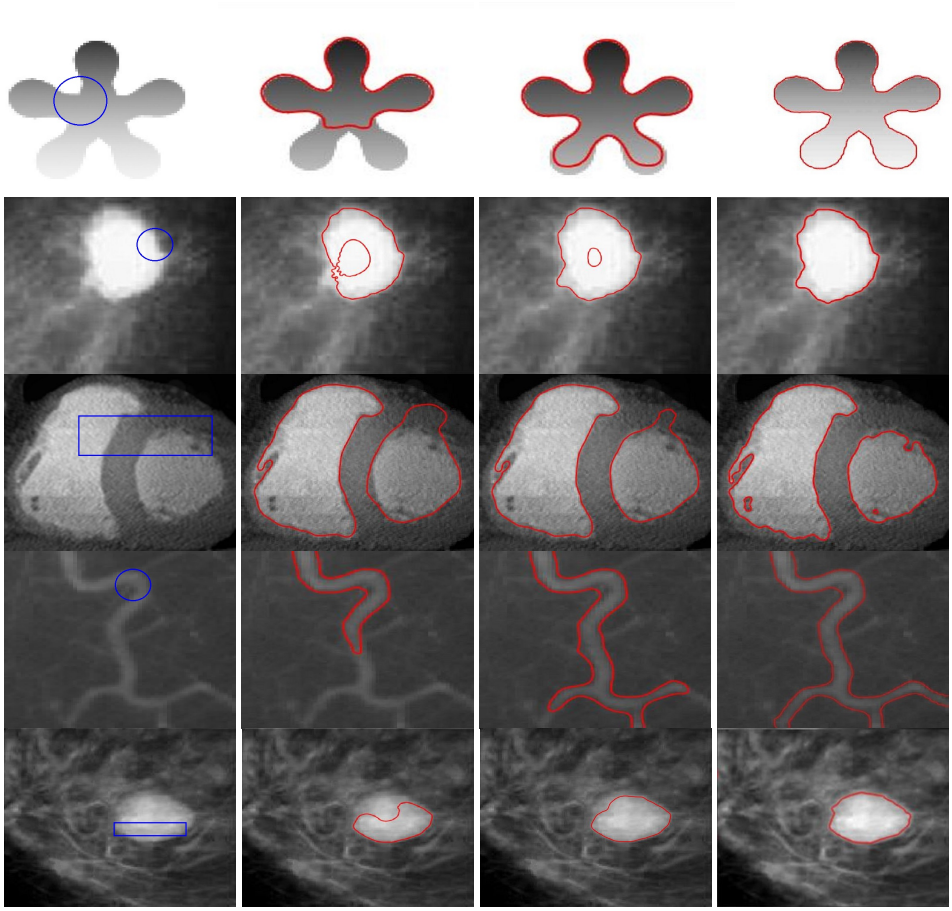

Figure 1. Different synthetic and medical images: column 1 = original images with different initial contour positions, column 2 = results after 10 iterations, column 3 = results after 19 iterations, and column 4 = final results of the proposed method.

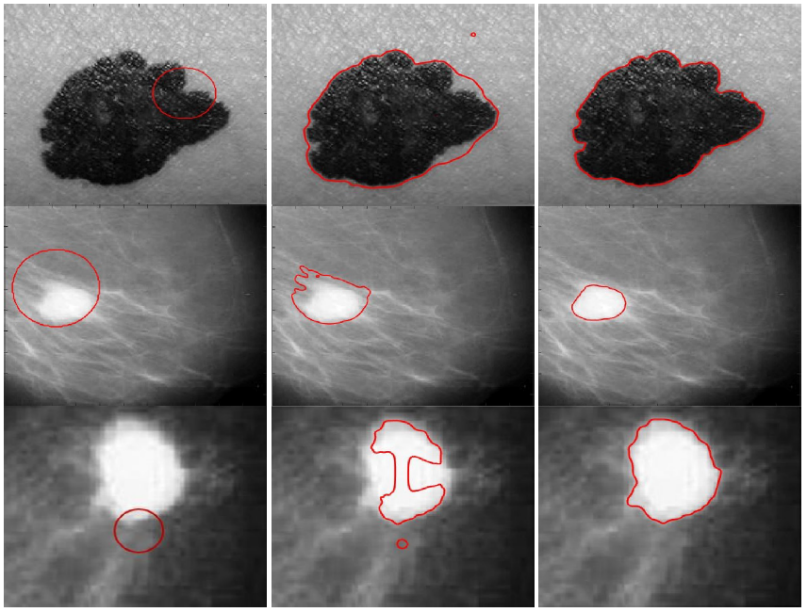

Figure 2. Medical images: column 1 = original images with initial contours, column 2 = proposed method after 10 iterations, and column 3 = final results using the proposed method.

This article has been accepted for publication in a future issue of this journal, but has not been fully edited. Content may change prior to final publication. Citation information: DOI 10.1109/ACCESS.2020.3034908, IEEE Access

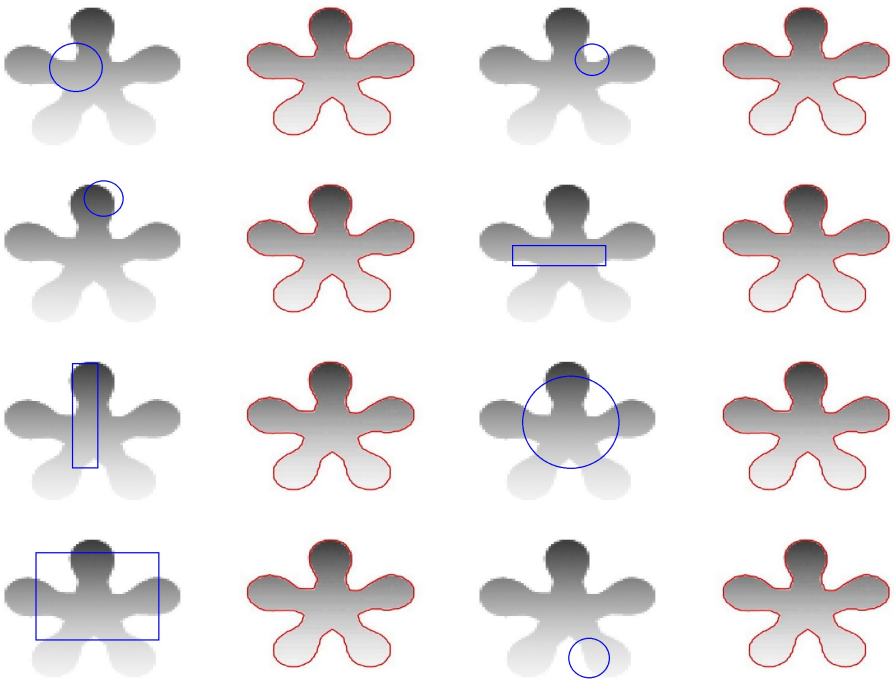

Figure 3. Synthetic images with different initial contour positions: columns 1 and 2 present the different initial contour positions, and columns 3 and 4 present the results using the proposed method.

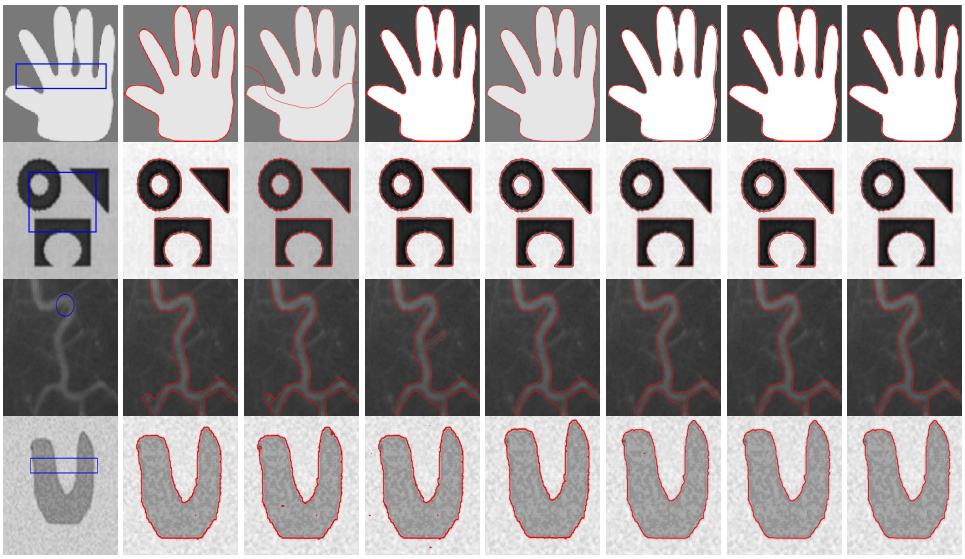

Figure 4. Synthetic images: column 1 = original images with initial contours, column 2 = LBF [4], column 3 = LIF [17], column 4 = VLSBC [25], column 5 = Min et al.'[29], column 6 = FRAGL [30], column 7 = LIFDG [31], and column 8 = proposed method.

This article has been accepted for publication in a future issue of this journal, but has not been fully edited. Content may change prior to final publication. Citation information: DOI 10.1109/ACCESS.2020.3034908, IEEE Access

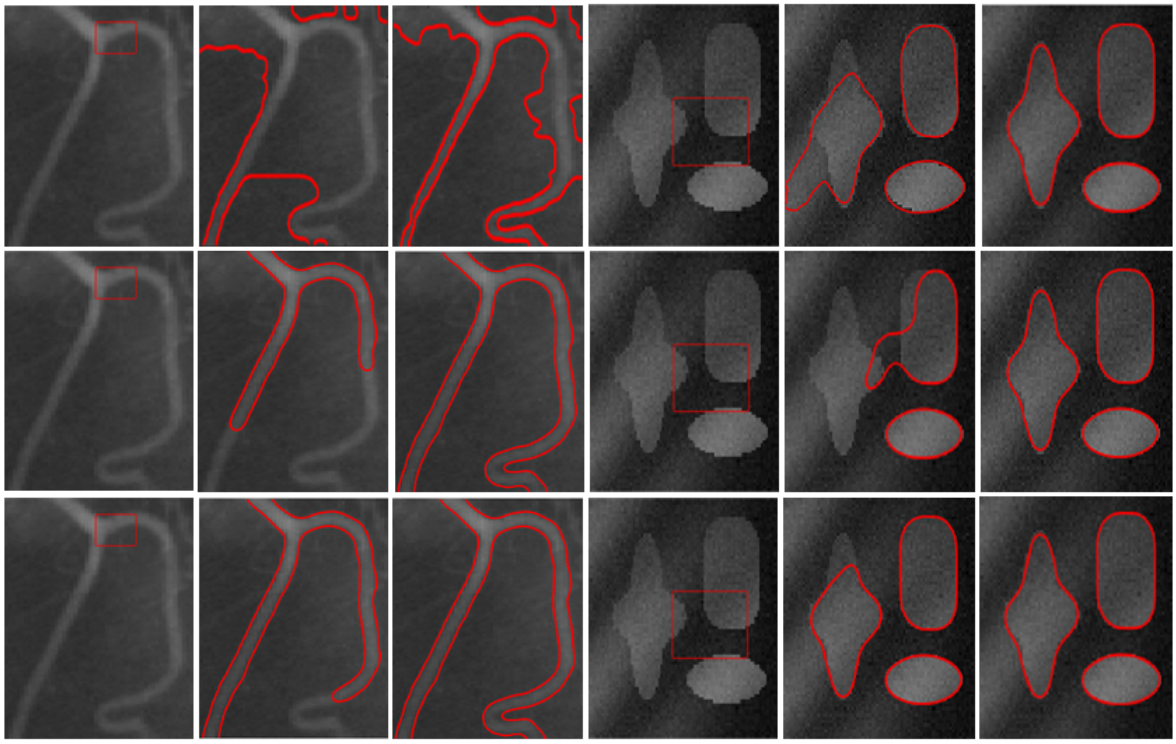

Figure 5. Segmentation results: The first row = WHRSPF [39], Second row = GLSEPF [40], Third row = Proposed method. Column 1 and 4 = origional image with initial contour, column 2 and 5 = results after 10 iteration, column 3 and 6 = final results.

Table 2. Segmentation accuracy of Figure 9.

	Methods					
Figure 5	LBF [4]	LIF [17]	VLSBC [25]	Min et al.'s [29]	FRAGL [30]	PM
Row 1	0.652	0.875	0.875	0.812	0.889	0.923
Row 2	0.235	0.248	0.628	0.684	0.878	0.935
Row 3	0.852	0.852	0.826	0.658	0.892	0.962
Row 4	0.752	0.713	0.758	0.487	0.925	0.972
Row 5	0.258	0.458	0.578	0.428	0.798	0.912

Table 3. Segmentation accuracy of Figure 11.

	Methods				
Figure 7	CV [3]	LBF [4]	Min et. al's [29]	FRAGL [30]	PM
Row 1	0.8398	0.9301	0.9293	0.9658	0.9754
Row 2	0.5601	0.8912	0.9125	0.9325	0.9712
Row 3	0.6878	0.8301	0.9325	0.9369	0.9831
Row 4	0.5784	0.8411	0.6523	0.9512	0.9812

row to the ninth row of each of the figures contains the segmentation results of three different Salt & Pepper noise levels: (0, 0.02, 0.04). The C-V [3] model results performed well in a few images; LBF [4] showed inferior segmentation results. Min et al. [29] fell in the local minima; however, it located the object boundaries. The FRAGL [30] and LIFDG [31] showed almost similar segmentation accuracy results to the proposed model.

Figure 7 demonstrates the segmentation results of different images with different levels of Gaussian noise. The top row to the ninth row of each of the figures contains the segmentation results of three different Gaussian noise levels: (0.01, 0.03, 0.04). The LBF [4] and VLSBC [25] models illustrated almost similar segmentation accuracy. FRAGL [30] and LIFDG [31] attained good performance and observed very near in segmentation accuracy to the proposed model. LIF [17] shows a false contour over the object boundaries. The proposed method segmented the RoI with the image complexity to make it robust to noise. The respective accuracy charts of Figures 6 and 7 are represented by images a and b in Figure 8.

This article has been accepted for publication in a future issue of this journal, but has not been fully edited. Content may change prior to final publication. Citation information: DOI 10.1109/ACCESS.2020.3034908, IEEE Access

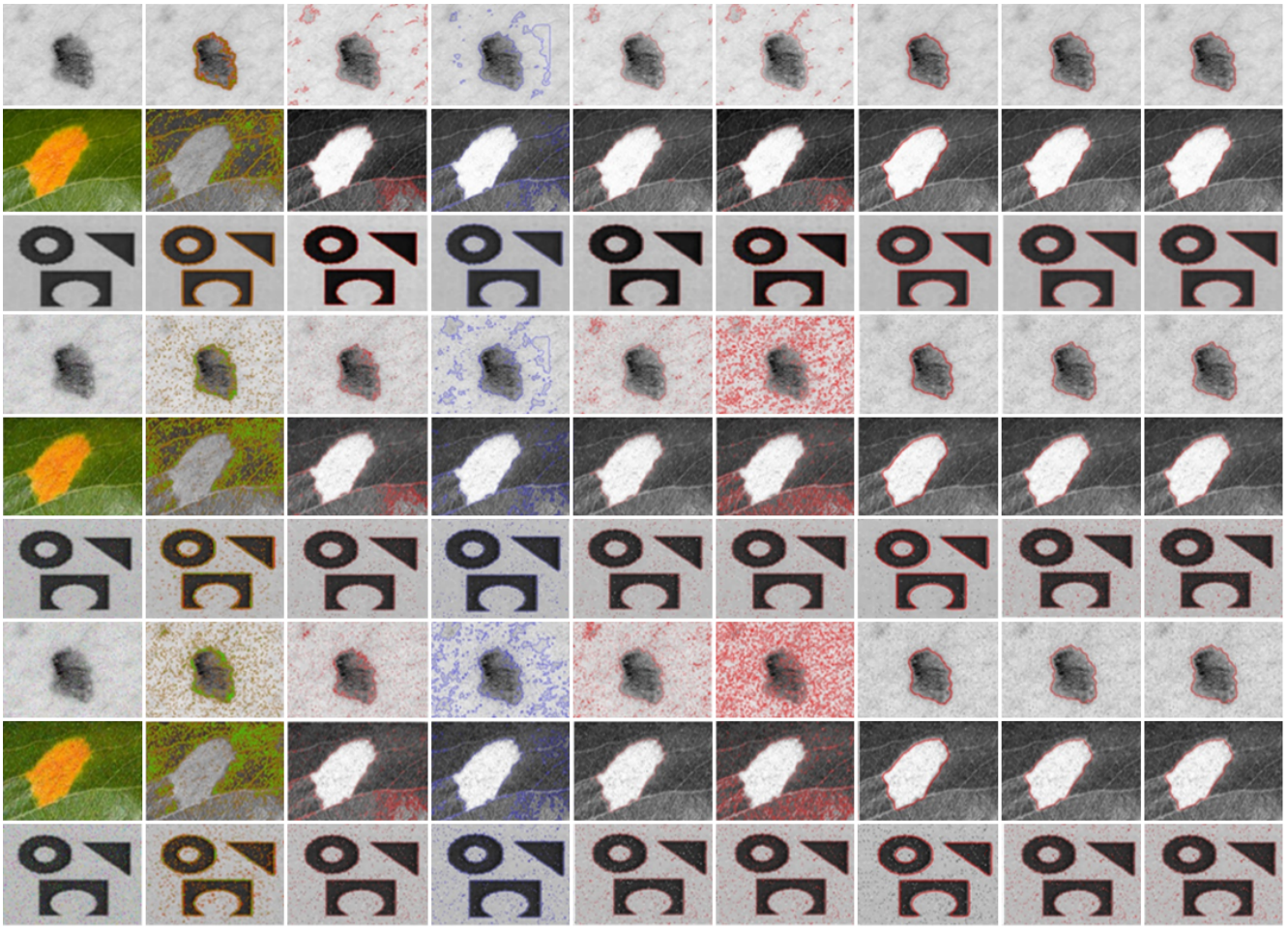

Figure 6. Left most column: Different inhomogeneous images with different levels of Salt & Pepper noise: (0, 0.02, 0.04); column 2 = C-V [3], column 3 = LBF method [4], column 4 = LIF method [17], column 5 = VLSBC method [25], column 6 = Min et al.[29], column 7 = FRAGL [30], column 8= LIFDG [31], and column 9 = proposed method.

V. QUANTITATIVE COMPARISON

The quantitative comparison is performed by measuring the Accuracy, Dice Index and Sensitivity for the mini-MIAS [34] database of mammograms, which include ROIs of different shapes and breast tumor X-rays. At first, experiments using the proposed method are performed with Synthetic color images to determine accuracy; the experiments' results were compared with those of previous models. The following metric is used for segmentation accuracy, Dice Index, and Sensitivity metrics are defined:

$$Accuracy = \frac{TP + TN}{TP + TN + FP + FN}, \tag{40}$$

$$DiceIndex = \frac{2 \times TP}{2 \times TP + FP + FN}, \tag{41}$$

and

$$Sensitivity = \frac{TP}{TP + FN}, \tag{42}$$

where TP defines the true-positive segmented regions, TN defines the true-negative unsegmented regions, FP defines the false positives inaccurately considered true, and FN defines false negatives, i.e., undetected object regions. Accuracy defines the segmented regions over the actual region. DSC is a dice coefficient, which defines the detected region's overlapping with the actual regions, and the Sensitivity detects the region belongs to the actual region.

Figure 9 illustrates the comparison of the results of the proposed method with the ground truth and previous models. Comparisons of the proposed method with ground truth and other state-of-the-art methods indicate that the LBF [4] and LIF [17] methods have weak segmentation results, whereas the VLSBC [25] model outperformed Min et al's model [29]. The FRAGL [30] had improved segmentation results, despite being weak in ignoring the noise in images. The proposed method had superior segmentation results and was nearer to the ground truth. Table 2 defines the comparisons in Figure 9, and a graphical representation of the comparisons is depicted in Figure 10. The proposed method demonstrated higher accuracy to the ground truth than previous methods.

This article has been accepted for publication in a future issue of this journal, but has not been fully edited. Content may change prior to final publication. Citation information: DOI 10.1109/ACCESS.2020.3034908, IEEE Access

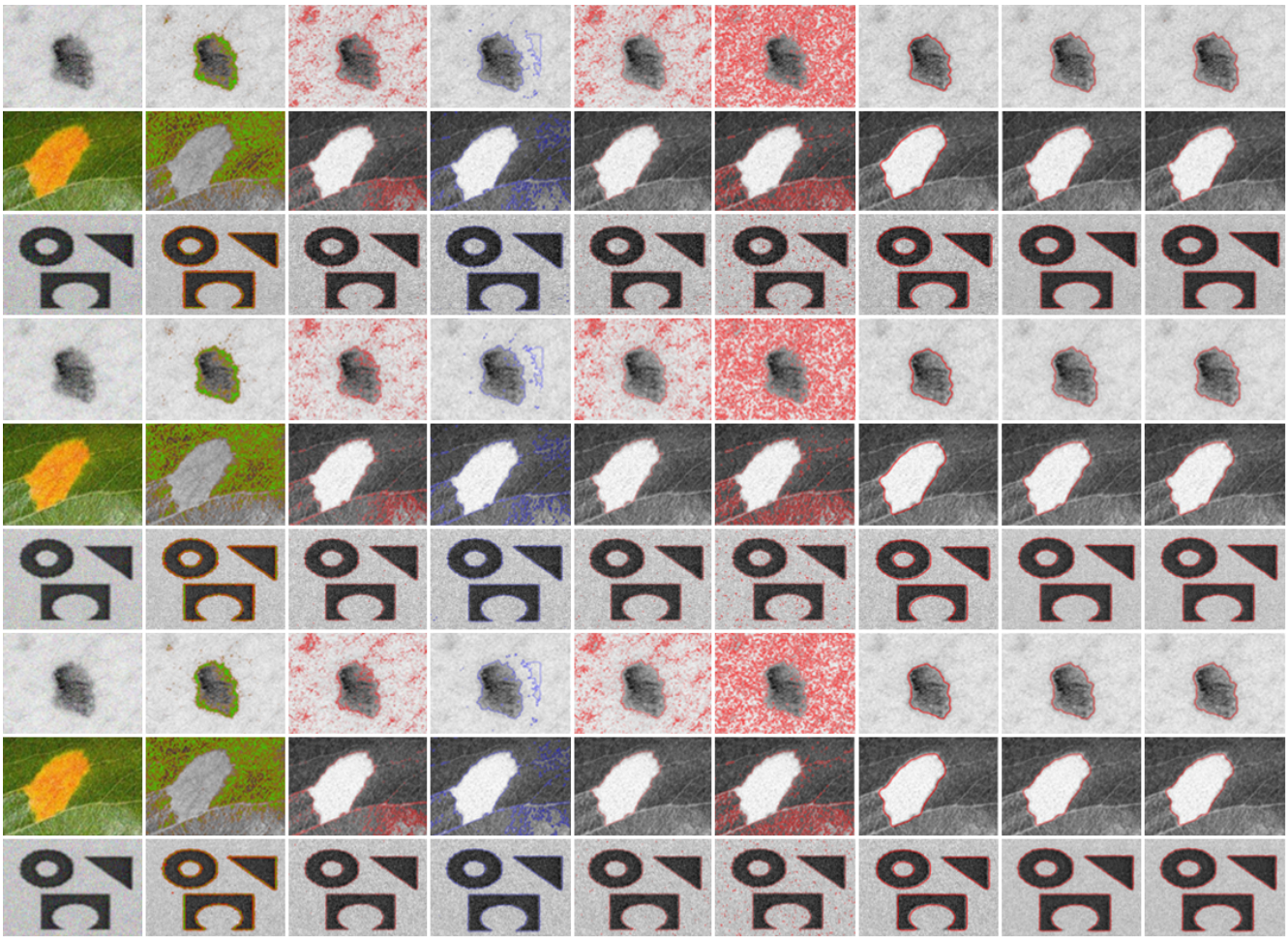

Figure 7. Left most column: Different inhomogeneous images with different levels of Gaussian noise: (0.01, 0.03, 0.04); column 2 = C-V [3], column 3 = LBF method [4], column 4 = LIF method [17], column 5 = VLSBC method [25], column 6 = Min et al.[29], column 7 = FRAGL [30], column 8= LIFDG [31], and column 9 = proposed method.

Figure 11 illustrates the publicly accessible mini-MIAS database [34] to confirm the segmentation accuracy of the proposed method. Table 3 defines the accuracy of the images while Figure 12 illustrates the graphical representation of the accuracy of Figure 11. Table 4 and Figure 13 depict the average number of iterations and average CPU times. Figure 12 illustrates the segmentation accuracy of the proposed method is significantly higher than the other previous methods.

A. DISCUSSION

The exiting ACMs define their formulations to construct objects in an image with local and global energy fitting. However, the proposed energy function defines the KD technique; it also combines an upgraded SPF Model to define global and local image information for inhomogeneous image segmentation. The proposed energy function combines the advantages of previous methods to generate a new method that is more effective for weak edges of objects, more accurate, and more time-efficient. The noise sensitivity analysis approves the proposed method results have improved accuracy compared with other methods. The average processing time and average number of iterations are presented in Table 4. Figure 12 illustrates the comparison outcomes of the images. The segmented results of different inhomogeneous intensity images corroborate the accuracy of the proposed method with fewer iterations comparatively to all other best practice level set approaches. The efficiency of deep learning image segmentation models, based on the training sample data set, also has more massive and more extensive data sets that tend to produce better accuracy and segmentation efficiency. Comparatively, supervised learning tends to produce inferior results on small datasets. However, the unsupervised level set methods perform segmentation using preselected parameters based on ROI. The proposed method sets the effective parameters to capture the ROI in images.

B. THE PARAMETERS

K is the KD operator and has a significant role in enabling the proposed model to segment objects with weak edges. In this study, the KD operator was combined with the upgraded SPF function to segment local and global image information and control the contour evolution process using the balloon

This article has been accepted for publication in a future issue of this journal, but has not been fully edited. Content may change prior to final publication. Citation information: DOI 10.1109/ACCESS.2020.3034908, IEEE Access

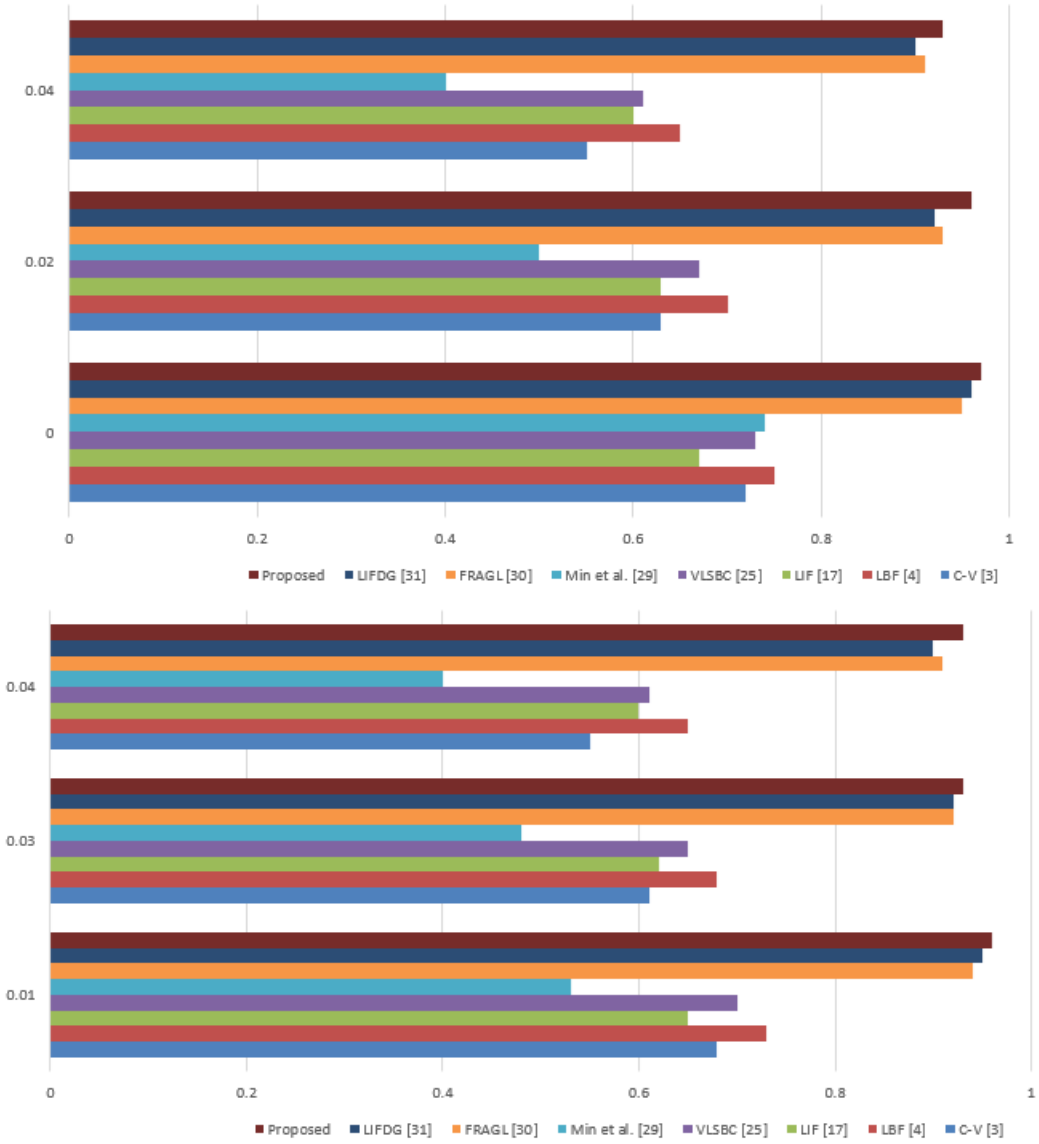

Figure 8. Jaccard Similarity (JS) values for Figure 7 and 8 are represtend by images a and b respectively.

Table 4. Average CPU time and number of iterations in Figure 10

Method	Average CPU Time	Average number of iterations
Chen-Vese [3]	5.993	31
LBF [4]	10.859	49
Min et. al's [29]	8.628	47
FRAGL [30]	4.897	36
Proposed	2.997	21

force.

VI. CONCLUSION

This paper proposed a new ACM based on KD and an upgraded SPF model to conduct image segmentation irrespective of weak edges or intensity inhomogeneity . The proposed model uses the KD on the edge-fitting energy term to segment weak edges and to extract the object boundary. The local and global fitting terms were combined to integrate the advantageous features of both terms for effective image segmentation. While the balloon force was used to facilitate the contour evolution process, the weight function was used to adjust weights between local and global information terms. The segmentation results with increased accuracy and decreased processing time are additional benefits of the proposed method . The quality of the proposed method was verified with experiments on synthetic and real images, including medical images. The image segmentation results and quantitative comparisons confirmed the contour initialization independence, high time efficiency, and superior segmentation accuracy of the proposed model in comparison to other segmentation models.

This article has been accepted for publication in a future issue of this journal, but has not been fully edited. Content may change prior to final publication. Citation information: DOI 10.1109/ACCESS.2020.3034908, IEEE Access

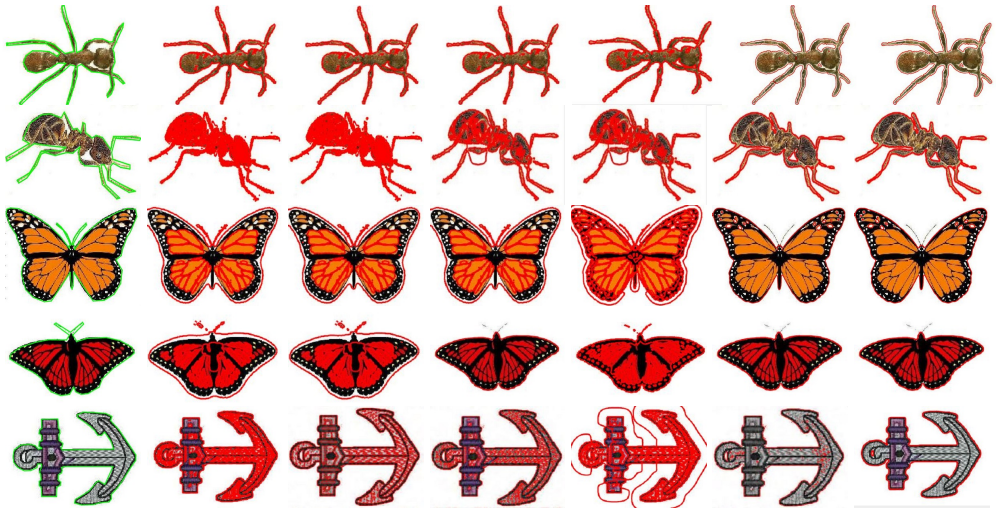

Figure 9. Synthetic color images: column 1 = original images with ground truth, column 2 = LBF [4], column 3 = LIF [17], column 4 = VLSBC [25], column 5 = Min et. al's [29], column 6 = FRAGL [30], and column 7 = proposed method.

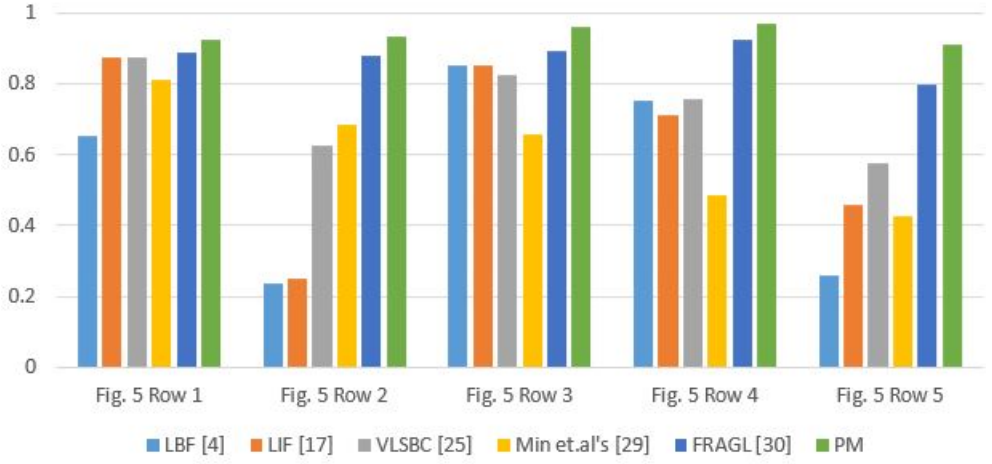

Figure 10. Segmentation accuracy graph for Figure 9

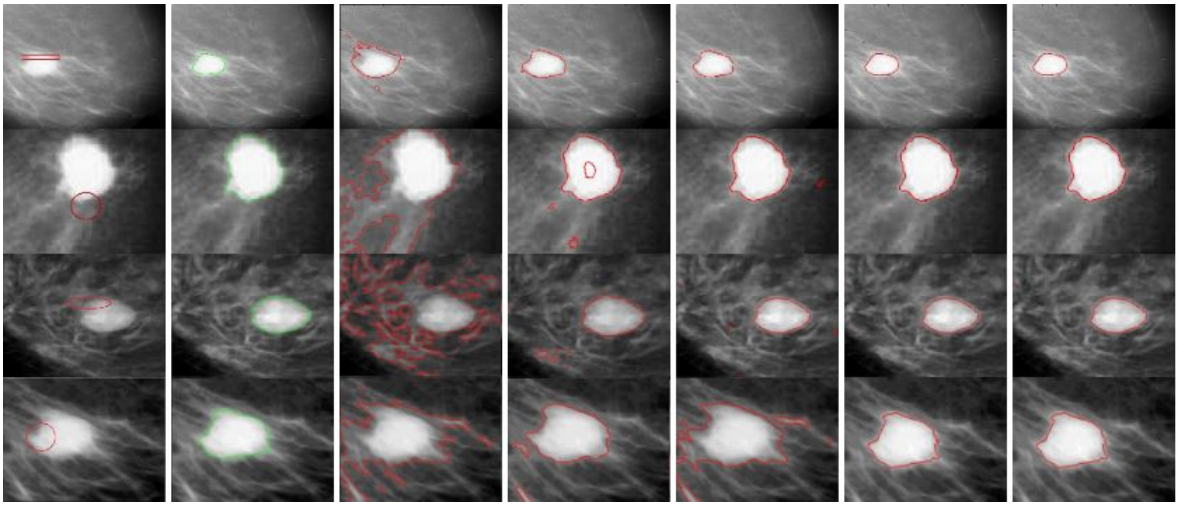

Figure 11. Typical mammogram images: column 1 = original images with initial contour, column 2 = ground truth, column 3 = CV [3], column 4 = LBF [4], column 5 = Min et al 's [29], column 6 = FRAGL [30], and column 7 = proposed method results.

This article has been accepted for publication in a future issue of this journal, but has not been fully edited. Content may change prior to final publication. Citation information: DOI 10.1109/ACCESS.2020.3034908, IEEE Access

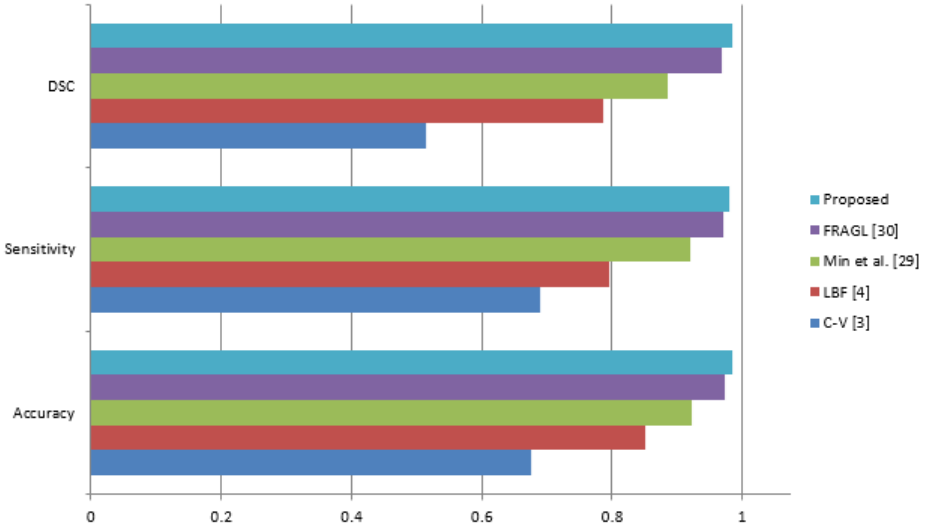

Figure 12. Metric analysis of the mini-MIAS dataset [34].

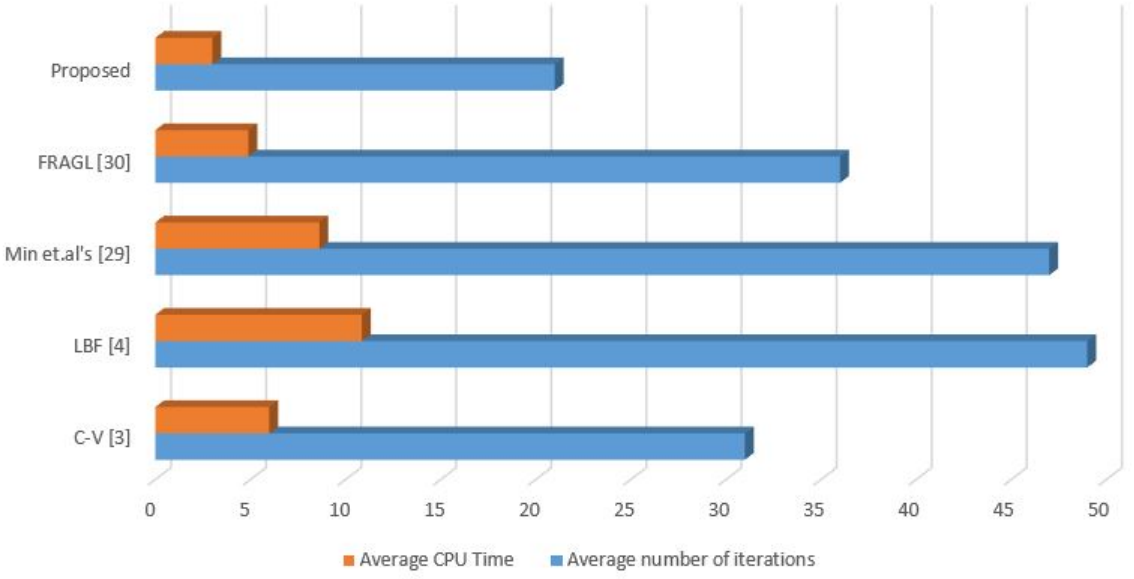

Figure 13. Average CPU time and number of iterations in Figure 11.

References

[1] C.-m. Li et al. "A level set method for image segmentation in the presence of intensity inhomogeneities with application to MRI," IEEE transactions on image processing, vol. 20, no. 7, pp. 2007–2016, 2011.

[2] J. C. Rajapakse, and F. Kruggel. "Segmentation of MR images with intensity inhomogeneities," Image and vision computing vol. 16, no. 3, pp. 165–180, 1998.

[3] T. F. Chan, and L. A. Vese. "Active contours without edges," IEEE Transactions on image processing, vol. 10, no. 2, pp. 266–277, 2001.

[4] C.-m. Li et al. "Minimization of region-scalable fitting energy for image segmentation," IEEE transactions on image processing, vol. 17, no. 10, pp. 1940–1949, 2008.

[5] L. A. Vese, and T. F. Chan. "A multiphase level set framework for image segmentation using the Mumford and Shah model," International journal of computer vision, vol. 50, no. 3, pp. 271–293, 2002.

[6] J. H. Kim et al. "Multipass active contours for an adaptive contour map," Sensors, vol. 13, no.3, pp. 3724–3738, 2013.

[7] D. Chen, M.-q. Yang, and L. D. Cohen. "Global minimum for a variant Mumford–Shah model with application to medical image segmentation," Computer Methods in Biomechanics and Biomedical Engineering: Imaging and Visualization, vol. 1, no. 1, pp. 48–60, 2013.

[8] X.-x. Huang, B. Huang, and H.-g. Li. "A fast level set method for synthetic aperture radar ocean image segmentation," Sensors vol. 9, no. 2, pp. 814–829, 2009.

[9] C.-m. Li, J.-d. Liu, and M.D. Fox. "Segmentation of edge preserving gradient vector flow: An approach toward automatically initializing and splitting of snakes," 2005 IEEE Computer Society Conference on Computer Vision and Pattern Recognition (CVPR'05). Vol. 1. IEEE, 2005.

[10] C.-m. Li, et al. "Level set evolution without re-initialization: a new variational formulation," 2005 IEEE computer society conference on computer vision and pattern recognition (CVPR'05). Vol. 1. IEEE, 2005.

[11] C.-m. Li et al. "Implicit active contours driven by local binary fitting energy." 2007 IEEE Conference on Computer Vision and Pattern Recognition, IEEE, 2007.

[12] M.-f. Huang et al. "A game-based economic model for price decision making in cyber-physical-social systems." IEEE Access, vol. 7, pp.

111559–111576, 2019.

[13] A. Tsai, A. Yezzi, and A, S. Willsky. "Curve evolution implementation of the Mumford-Shah function for image segmentation, denoising, interpolation, and magnification," IEEE transactions on Image Processing, vol. 10, no. 8, pp. 1169–1186, 2001.

[14] S. Soomro, A. Munir, and K. N. Choi. "Hybrid two-stage active contour method with region and edge information for intensity inhomogeneous image segmentation," PloS one, vol. 13, no. 1, 2018.

[15] H.-y. Xu et al. "A global and local active contour model based on dual algorithm for image segmentation," Computers Mathematics with Applications, vol. 74, no. 6, pp. 1471–1488, 2017.

[16] Z.-x. Ji et al. "Active contours driven by local likelihood image fitting energy for image segmentation," Information Sciences, vol. 301, pp. 285–304, 2015.

[17] K.-h. Zhang, H.-h. Song, and L. Zhang. "Active contours driven by local image fitting energy," Pattern recognition, vol. 43, no. 4, pp. 1199–1206, 2010.

[18] K.-h. Zhang et al. "Active contours based on image Laplacian fitting energy," Chinese Journal of Electronics, vol. 18, no. 2, pp. 281–284, 2009.

[19] Kass, Michael, Andrew Witkin, and Demetri Terzopoulos. "Snakes: Active contour models." International journal of computer vision 1.4 (1988): 321-331.

[20] L. Zhang et al. "A novel active contour model for image segmentation using local and global region-based information," Machine Vision and Applications, vol. 28, no. 1–2, pp. 75–89, 2017.

[21] Y. Tian et al. "Active contour model combining region and edge information," Machine vision and applications, vol. 24, no. 1, pp. 47–61, 2013.

[22] K. H. Lok et al. "Fast and robust brain tumor segmentation using level set method with multiple image information," Journal of X-ray Science and Technology, vol. 25, no. 2, pp. 301–312, 2017.

[23] K.-h. Zhang et al. "A level set approach to image segmentation with intensity inhomogeneity," IEEE transactions on cybernetics, vol. 46, no. 2, pp. 546–557, 2015.

[24] K.-h. Zhang et al. "Active contours with selective local or global segmentation: A new formulation and level set method," Image and Vision computing, vol. 28, no. 4, pp. 668–676, 2010.

[25] C.-m. Li et al. "A variational level set approach to segmentation and bias correction of images with intensity inhomogeneity," International Conference on Medical Image Computing and Computer-Assisted Intervention. Springer, Berlin, Heidelberg, 2008.

[26] Z. Sun et al. "Image segmentation by searching for image feature density peaks," Applied Sciences, vol. 8, no. 6, pp. 969, 2018.

[27] H.-y. Xu et al. "A global and local active contour model based on dual algorithm for image segmentation," Computers Mathematics with Applications, vol. 74, no. 6, pp. 1471–1488, 2017.

[28] M. M. Abdelsamea, and S. A. Tsaftaris. "Active contour model driven by globally signed region pressure force," 2013 18th International Conference on Digital Signal Processing (DSP). IEEE, 2013.

[29] H. Min et al. "An intensity-texture model-based level set method for image segmentation," Pattern Recognition, vol. 48, no. 4, pp. 1547–1562, 2015.

[30] J.-x. Fang et al. "Fuzzy region-based active contours driven by weighting global and local fitting energy," IEEE Access, 2019.

[31] Y.-x. Duan, T.-l. Peng, and X.-h. Qi. "Active contour model based on LIF model and optimal DoG operator energy for image segmentation," Optik, vol. 202, 2020, 163667.

[32] A. Niaz et al. "Hybrid Active contour Based on Local and Global Statistics Parameterized by Weight Coefficients for Inhomogeneous Image Segmentation," IEEE Access, vol. 8, pp. 57348–57362, 2020.

[33] S. Soomro, T. A. Soomro, and K. N. Choi. "An active contour model based on region based fitting terms driven by p-Laplace length regularization." IEEE Access, vol. 6, pp. 58272–58283, 2018.

[34] The mini-MIAS database of mammograms, available at: http://peipa.essex.ac.uk/info/mias.html

[35] Willcocks, Chris G., et al. "Interactive GPU active contours for segmenting inhomogeneous objects." Journal of Real-Time Image Processing 16.6 (2019): 2305-2318.

[36] Abdelsamea, Mohammed M., Giorgio Gnecco, and Mohamed Medhat Gaber. "An efficient Self-Organizing Active Contour model for image segmentation." Neurocomputing 149 (2015): 820-835.

[37] Yu, Haiping, Fazhi He, and Yiteng Pan. "A novel segmentation model for medical images with intensity inhomogeneity based on adaptive perturbation." Multimedia Tools and Applications 78.9 (2019): 11779-11798.

[38] Abdelsamea, Mohammed M., Giorgio Gnecco, and Mohamed Medhat Gaber. "A SOM-based Chan–Vese model for unsupervised image segmentation." Soft Computing 21.8 (2017): 2047-2067.

[39] Fang, Jiangxiong, et al. "Active contour driven by weighted hybrid signed pressure force for image segmentation." IEEE Access 7 (2019): 97492-97504.

[40] Liu, Huaxiang, et al. "A Novel Active Contour Model Guided by Global and Local Signed Energy-Based Pressure Force." IEEE Access 8 (2020): 59412-59426.

[41] Han, Bin, and Yiquan Wu. "Active contours driven by global and local weighted signed pressure force for image segmentation." Pattern Recognition 88 (2019): 715-728.

[42] Yu, Yang, et al. "Active contour method combining local fitting energy and global fitting energy dynamically." International Conference on Medical Biometrics. Springer, Berlin, Heidelberg, 2010.

[43] Tiwari, Arti, Shilpa Srivastava, and Millie Pant. "Brain tumor segmentation and classification from magnetic resonance images: Review of selected methods from 2014 to 2019." Pattern Recognition Letters 131 (2020): 244-260.

ASIF AZIZ MEMON received his B.E. degree from Mehran UET, Jamshoro, Pakistan, in 2010, M.E. degree from Mehran UET, Jamshoro, Pakistan, in 2015, and is currently pursuing a Ph.D. degree in Application Software from Chung-Ang University, Seoul, South Korea.

Since 2018, he is working as a Research Assistant with the Visual Image Media Lab, Chung-Ang University, Seoul, South Korea, under Prof. Dr. Choi. His research interests include image segmentation, image recognition, and medical imaging.

ASIM NIAZ received his B.S. degree in electrical (computer) engineering from COMSATS Institute of Information Technology, Pakistan, in 2016. His M.S. from the Department of Computer Science and Engineering of Chung-Ang University, South Korea.

Currently, he is a researcher with the STARS team at INRIA Sophia Antipolis. His area interests are action recognition, video understanding, medical image analysis, and image segmentation.

SHAFIULLAH SOOMRO received a B.E. from QUEST, Nawabshah, Pakistan in 2008, his M.E. from MUET, Jamshoro, Pakistan in 2014, and his Ph.D. in Computer Science from Chung-Ang University, Seoul, South Korea in 2018.

He is currently an Assistant Professor in Computer Science at the Quaid-e-Awam University of Engineering, Science and Technology (QUEST), Shaheed Benazirabad, Pakistan. His research interests include motion tracking, object segmentation, and 3-D image recognition.

EHTESHAM IQBAL received his B.S. in Electrical (Computer) Engineering from the COMSATS Institute of Information Technology, Pakistan in 2017.

Since 2019, He is working as a Research Assistant with the Visual Image Media Lab, Chung-Ang University, Seoul, South Korea, under Prof. Dr. Choi. His current research interests include medical image analysis, semantic segmentation, and generative modeling.

ASAD MUNIR received the bachelor's degree in engineering sciences from GIK Institute, Pakistan, in 2013, and the master's degree in computer science from Chung-Ang University, South Korea, in 2018.

He is currently pursuing the Ph.D. degree with the Department of Industrial and Information Engineering, Università degli Studi di Udine, Italy. His current research interests include object segmentation, object tracking, and person re-identification.

KWANG NAM CHOI received B.S. and M.S. degrees from the Department of Computer Science, Chung-Ang University, Seoul, South Korea, in 1988 and 1990, respectively, and a Ph.D. degree in computer science from the University of York, U.K., in 2002.

He is currently a Professor with the School of Computer Science and Engineering, Chung-Ang University. His current research interests include motion tracking, object categorization, and 3D image recognition.